Figure 1. Mouse model of chronic aristolochic acid nephropathy (AAN). (A) Workflow of the animal model used. Aristolochic acid (2.5 mg/kg) was administered i.p. on 4 occasions on days 0, 3, 7 and 10. (B) Significant difference of serum creatinine at the end of the experiment (n=7 in each group). (C) Masson's Trichrome stain of kidneys from health mouse (left, Naïve) and mouse with chronic AAN (right, AAN) taken at day 28. Cytoplasm in stained red, collagen in blue and nuclei are in dark brown that helps to identify renal fibrosis. Significant fibrotic changes developed in mouse kidney due to AAN. (D) (E) (F) Immunohistochemistry stain of Ki67, alpha-SMA and HAVCR1 for Naïve/AAN kidneys. Micrographs shown are representative of 4 naïve mice and 4 AAN mice. (G) (H) Quantification of collagen (cyan signal) in Masson's Trichrome stain and alpha-smooth muscle actin DAB signal were used to confirm fibrosis in the AAN model. (I) Nuclear Ki67 DAB signal was used to quantify proliferating cells as a percentage of all hematoxylin stained cells. (Scale bar = 50μm)

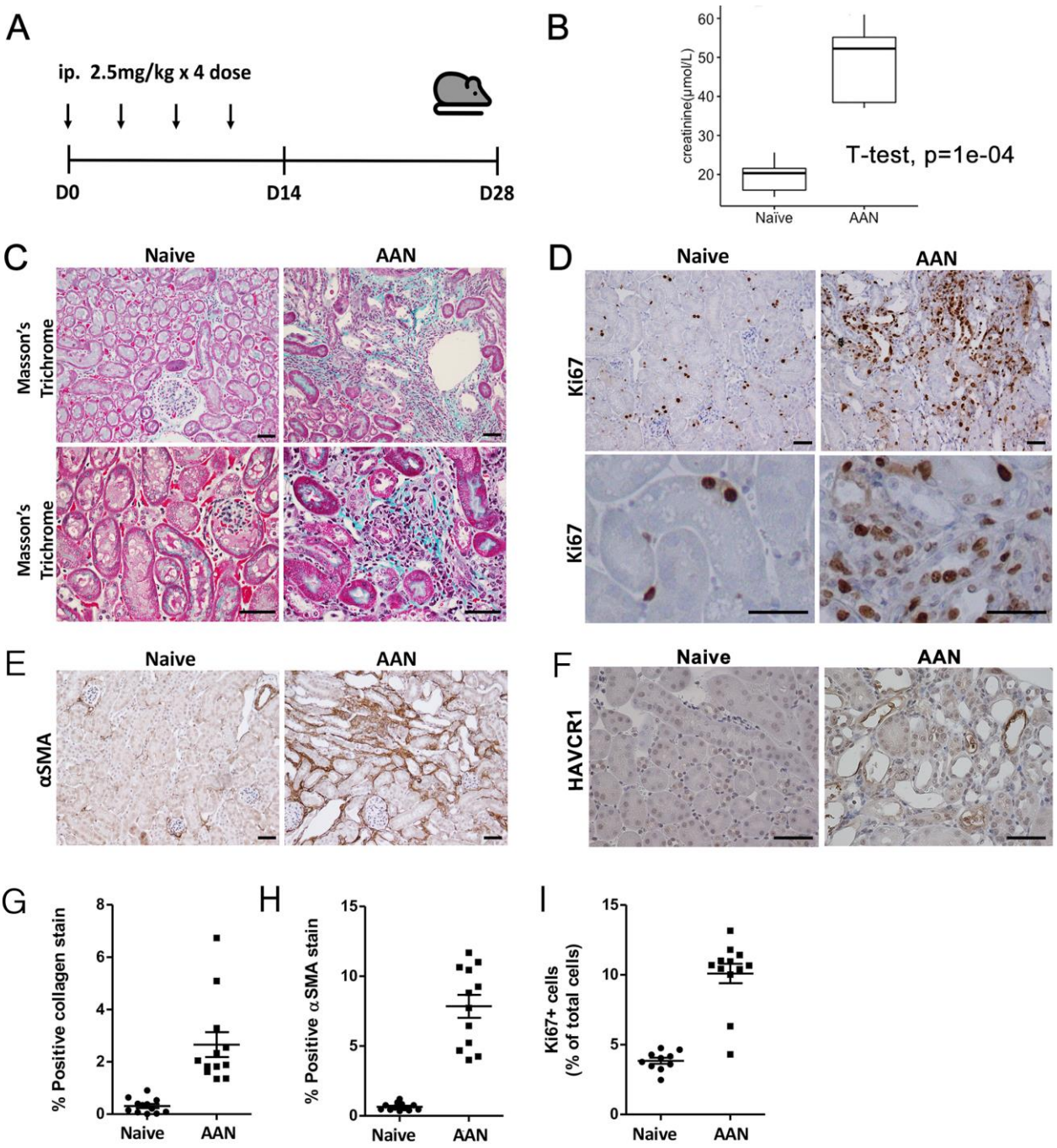

Figure 2. Clustering and cell-type identification of 23,885 nuclei using combined datasets from four naïve and four AAN mice. (A) Uniform manifold approximation and projection (UMAP) plot of the combined dataset is shown by splitting conditions. We identified all major cell types in kidney and four new classes of cells, labeled as proliferative cell and New-PT clusters 1-3. (B) Dotplot shows the expression levels and the percentage of gene expression of the canonical genes in each distinct cell type. (C) Feature plot of regional-specific genes shows the expression of *Cyp2e1* (purple) in cortical PTCs and *Cyp7b1* (green) in medullary PTCs. (D) Expression of canonical genes of principal cells (PCs) in outer and inner medullary collecting duct shows the PCs from the two different regions were well-clustered.
JG cell, Juxtaglomerular cells; PT, proximal tubule; S1/S2/S3, segment 1/2/3 of proximal tubule; DTL, descending thin limb; ATL, ascending thing limb; TAL, thick ascending limb; DCT1/DCT2, distal convoluted tubule1/2; CNT, connecting tubule; PC-OMCD, principal cell-outer medullary collecting duct; PC-IMCD, principal cell-inner medullary collecting duct; IC-A, intercalated cells, type A; IC-B, intercalated cells, type B.

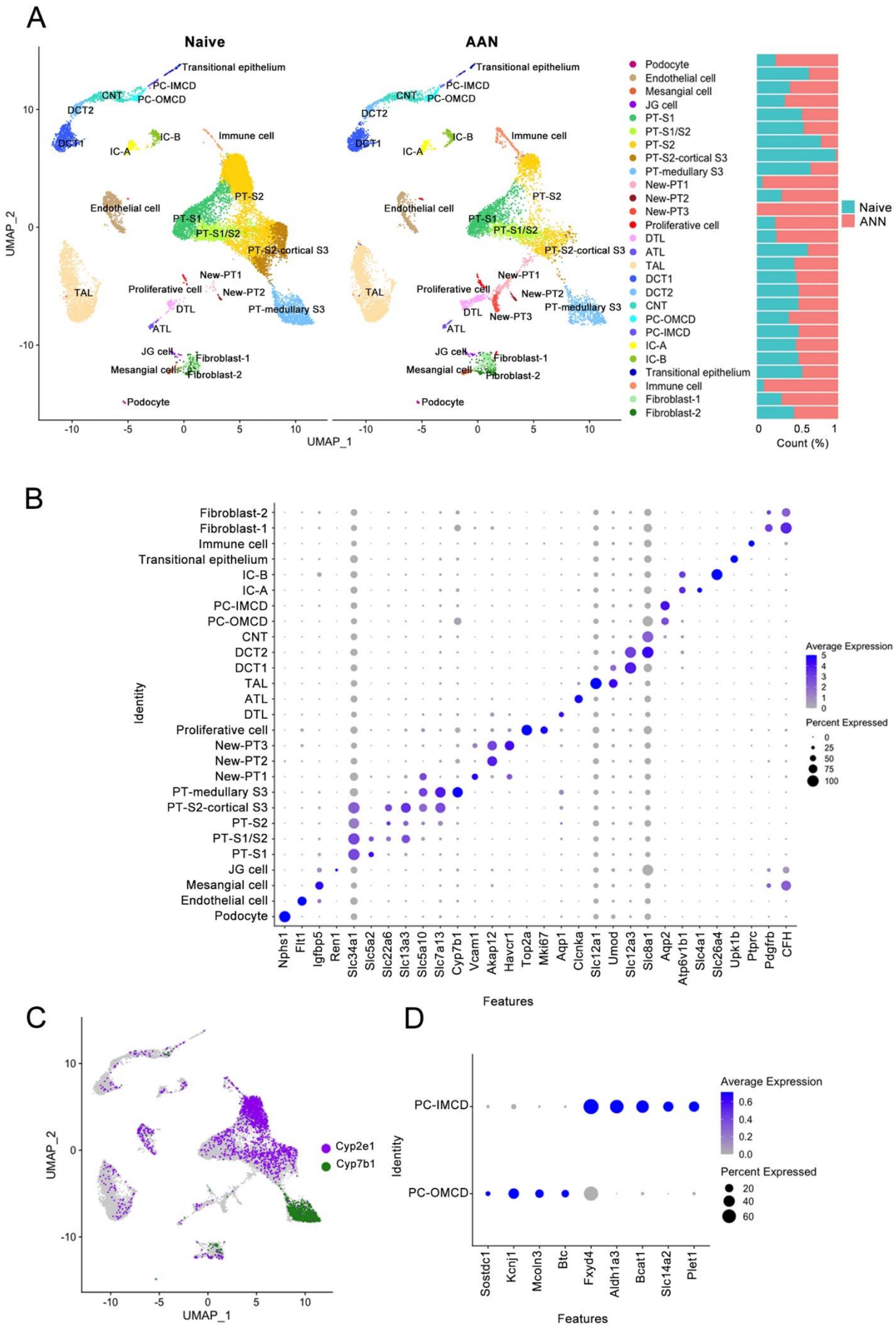
A
Naive
AAN
Transitional epithelium
PC-IMCD
CNT
PC-OMCD
DCT2
DCT1
IC-A
IC-B
Immune cell
Endothelial cell
PT-S2
PT-S1
PT-S1/S2
PT-S2-cortical S3
New-PT1
Proliferative cell
New-PT2
TAL
DTL
PT-medullary S3
New-PT3
ATL
JG cell
Fibroblast-1
Mesangial cell
Fibroblast-2
Podocyte
UMAP_1
UMAP_2
Naive
ANN
Count (%)
B
Identity
Features
Average Expression
Percent Expressed
Nphs1
Flt1
Igfbp5
Ren1
Slc34a1
Slc5a2
Slc22a6
Slc13a3
Slc5a10
Slc7a13
Cyp7b1
Vcam1
Akap12
Havcr1
Top2a
Mki67
Aqp1
Clcnka
Slc12a1
Umod
Slc12a3
Slc8a1
Aqp2
Atp6v1b1
Slc4a1
Slc26a4
Upk1b
Ptprc
Pdgfrb
CFH
C
Cyp2e1
Cyp7b1
D
PC-IMCD
PC-OMCD
Sostdc1
Kcnj1
Mcoln3
Btc
Fxyd4
Aldh1a3
Bcat1
Slc14a2
Plet1

Figure 3. Gene expression profiles of Proximal Tubular Cell clusters. (A) Dotplot shows the expression levels and the percentage of gene expression in each cluster of the canonical genes in the normal and new classes of PTCs. (B) (C) (D)Volcano plots show the significant genes in differentially expressed gene analysis of the three New-PT clusters by comparing the RNA profiles of one cluster to all other clusters of the dataset. Significance was defined as a gene with an adjusted p value < 0.05, a ≧ 0.25 average log fold difference between the two groups of cells, and with presence detected in at least 10% of cells in either of the two populations.

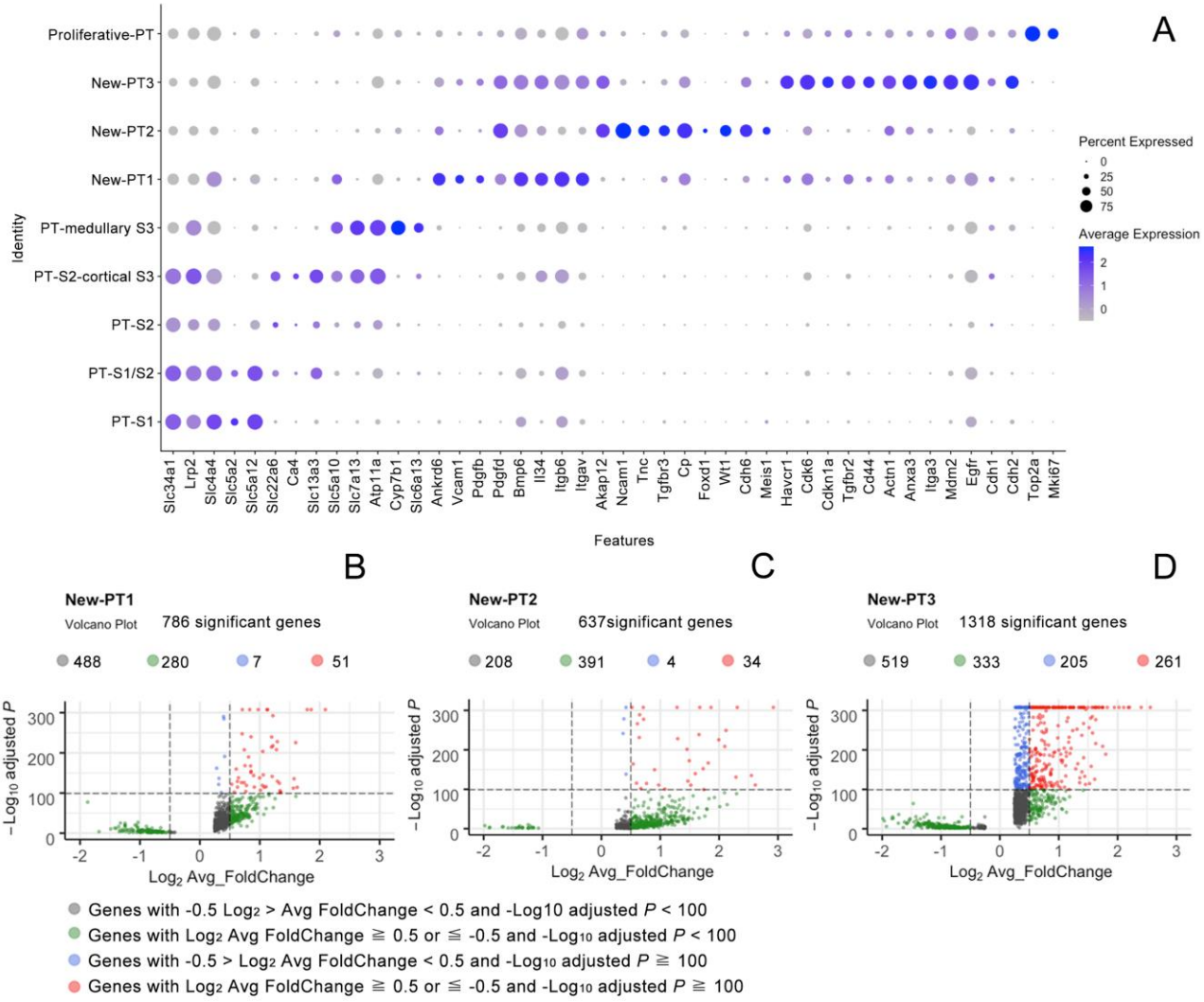

Figure 4. Trajectory, RNA velocity and pseudotime analysis of the Proximal Tubular Cells. (A) Trajectory analysis shows dynamic process of the PTCs. RNA expression profiles change continuously along the anatomic axis in normal PTCs (PT-S1 to PT-S3). (B) RNA velocity analysis shows New-PT1 is an intermediate cell type that may differentiate toward two directions "New-PT1 – New-PT2 - proliferative PT - normal PTCs and "New-PT1 – New-PT3". The New-PT 1-3 and the proliferative PTCs are more likely to differentiation and the normal PTs are the mature populations (C) PTC pseudotime analysis.

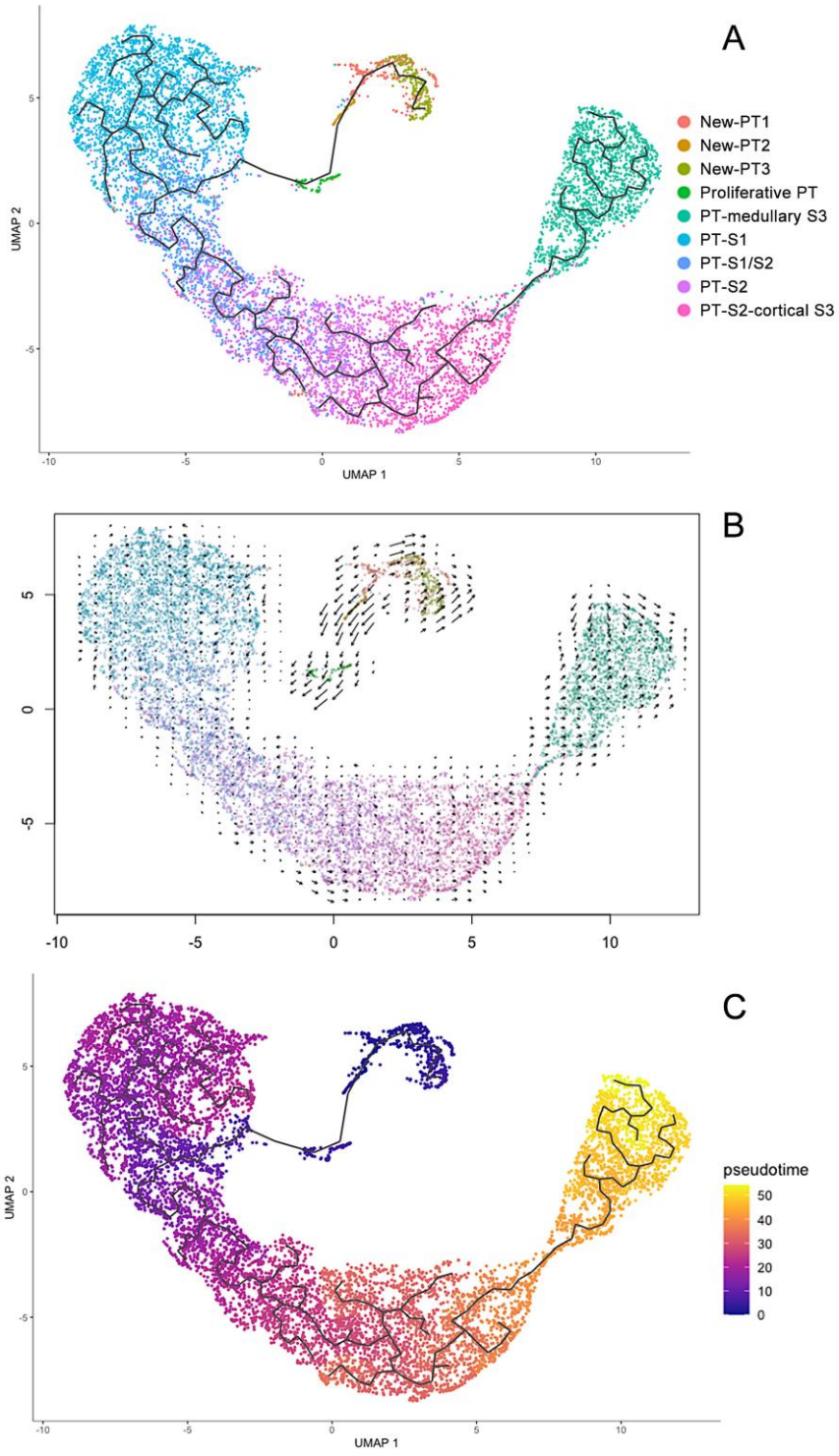

Figure 5 Immunofluorescence stain of the New-PT clusters. Co-staining of sections from Naïve and AAN kidneys for, (A-B) SLCA4 and VCAM1, (C-D) HAVCR1 and P21, (E-H) Foxd1 and Akap12, (I-L) Foxd1 and WT1 (Scale Bar =20μm). (F, H, J, L) Foxd1, Akap12, WT1 were detected in glomeruli as well as tubulointerstitium

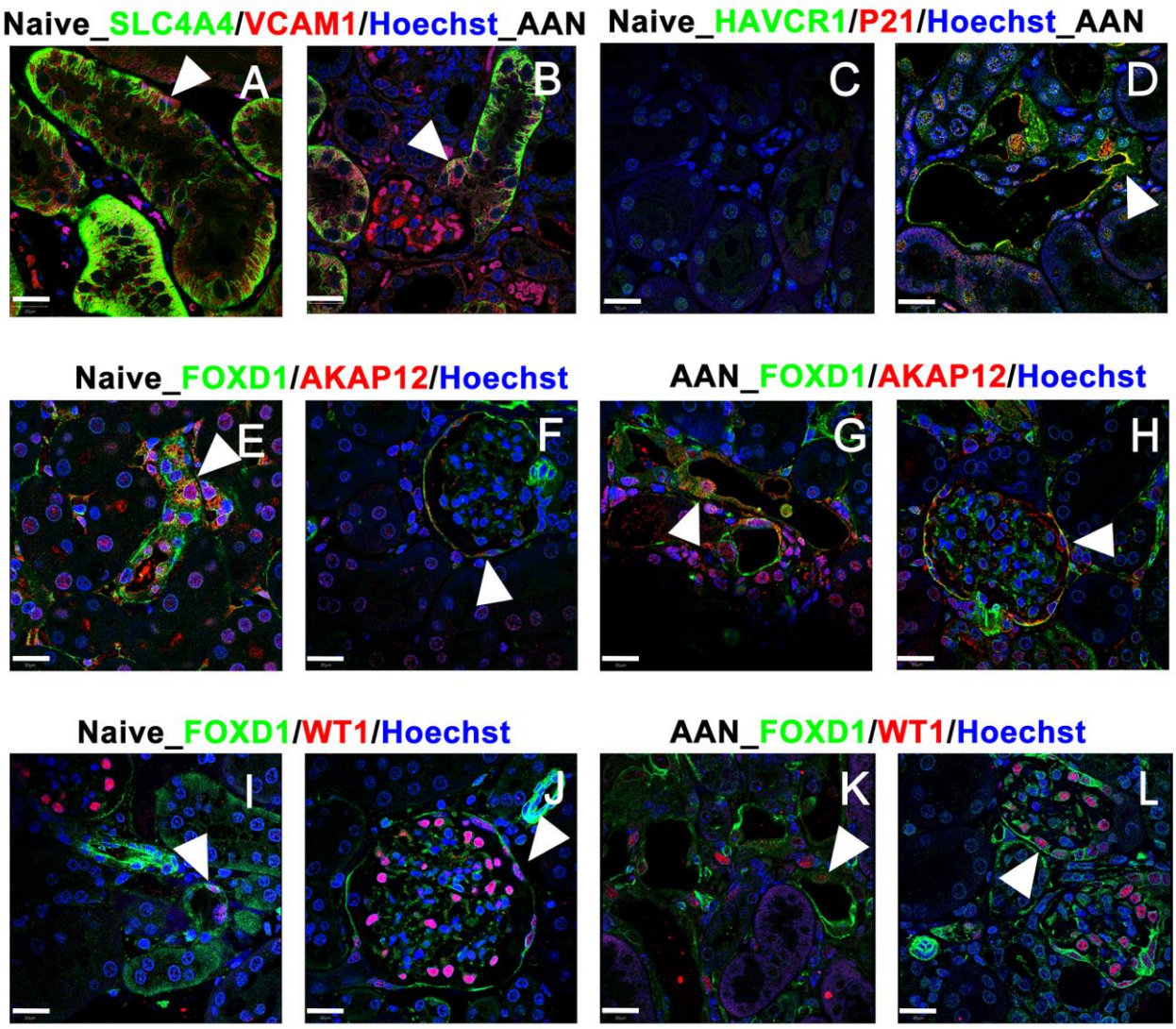

Figure 6. Pathway analysis based on KEGG database. Results shows metabolic reprogramming, enrichment of cellular communication and cell motility, and various immune activations in New-PT clusters. The enrichment was calculated by comparing the RNA profiles of one New-PT cluster to all other PTC clusters. Pathways with a false discovery rate < 0.25 were listed.

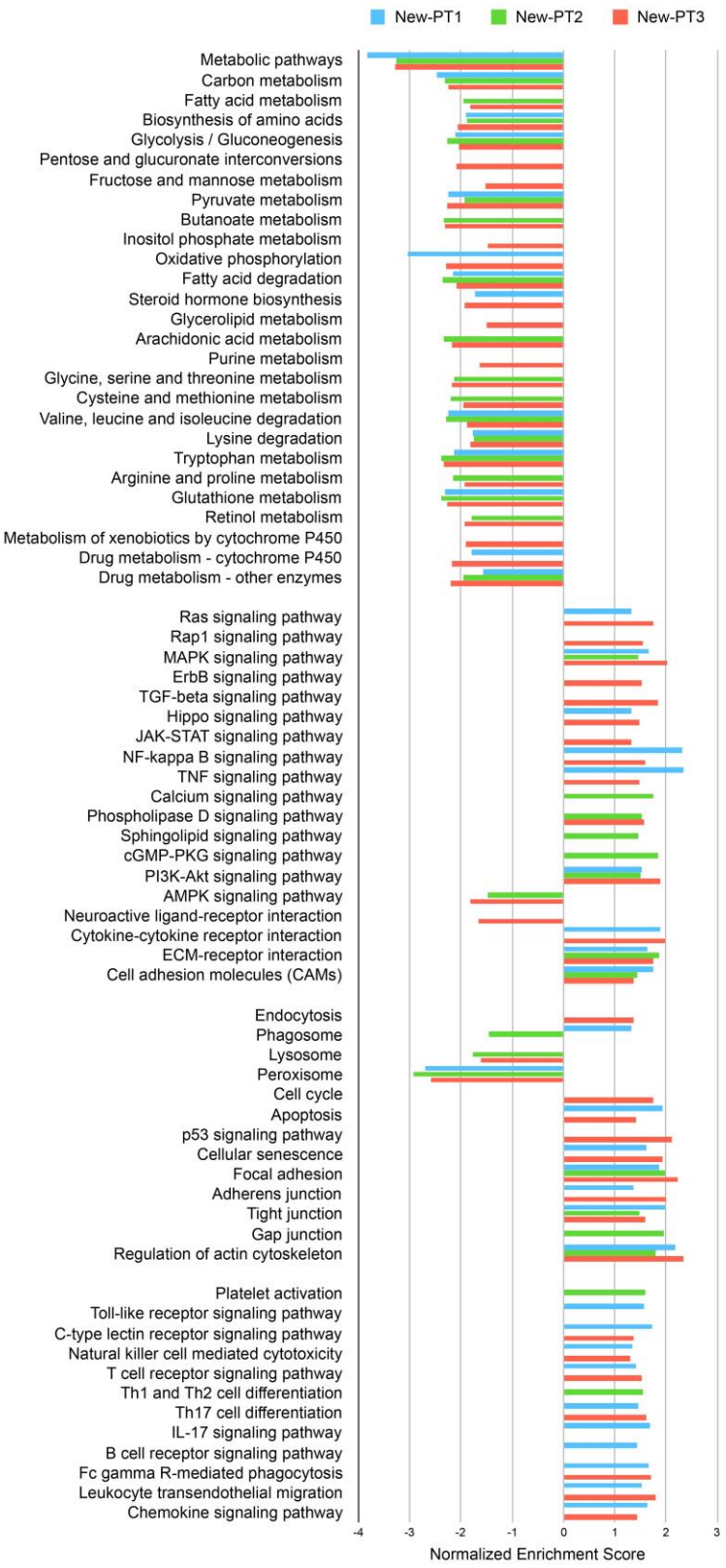

Figure 7. Ligand-receptor analysis. (A) PT S1-S3 are combined to normal PT and fibroblast-1, 2 are combined to Fibroblast for ligand-receptor analysis. Heatmap shows the cross product of ligand gene expression from normal PT, New-PT1, New-PT2, New-PT3 and receptor gene expression from (B) fibroblast, (C) immune cells, (D) normal PT..